Geophysical Research Letters

RESEARCH LETTER
10.1029/2023GL104795

Evidence for the Presence of Thin and Heterogenous Dust Deposits on Ryugu's Boulders From Hayabusa2 MARA and Sample Data

M. Hamm[1,2], V. E. Hamilton[3], and C. A. Goodrich[4]

[1]Freie Universität Berlin, Berlin, Germany, [2]Institute of Planetary Research, German Aerospace Center (DLR), Berlin, Germany, [3]Southwest Research Institute, Boulder, CO, USA, [4]Lunar and Planetary Institute, Houston, TX, USA

Key Points:

- The Ryugu sample C0137's mid-IR spectrum shows differences to in-situ observations by MARA
- The differences can be explained by the presence of dust on the boulders of Ryugu
- Thermal modeling reveals that dust covering less than 3% of the MARA field of view is consistent with the MARA data

Correspondence to:

M. Hamm,
maximilian.hamm@dlr.de

Citation:

Hamm, M., Hamilton, V. E., & Goodrich, C. A. (2023). Evidence for the presence of thin and heterogenous dust deposits on Ryugu's boulders from Hayabusa2 MARA and sample data. *Geophysical Research Letters*, *50*, e2023GL104795. https://doi.org/10.1029/2023GL104795

Received 2 JUN 2023
Accepted 24 OCT 2023

Author Contributions:

Conceptualization: M. Hamm, V. E. Hamilton, C. A. Goodrich
Data curation: V. E. Hamilton, C. A. Goodrich
Formal analysis: M. Hamm
Funding acquisition: M. Hamm, V. E. Hamilton, C. A. Goodrich
Investigation: V. E. Hamilton, C. A. Goodrich
Methodology: M. Hamm, V. E. Hamilton, C. A. Goodrich
Software: M. Hamm
Supervision: V. E. Hamilton
Validation: M. Hamm
Writing – original draft: M. Hamm
Writing – review & editing: V. E. Hamilton, C. A. Goodrich

Abstract Middle infrared spectral results obtained in-situ by the Hayabusa2 MARA instrument are generally in-line with previous results and a new comparison with sample C0137 returned from asteroid (162173) Ryugu, being similar to an aqueously altered CI1 chondrite. The mid-IR spectrum of the boulder on Ryugu measured by MARA is shallower around 9 μm compared to the laboratory spectrum of C0137. Here we show that discontinuous, fine dust deposits can partially explain the differences in the spectral data and remain in agreement with the temperature observations of the boulder by MARA if an opaque dust layer covers less than 3% of the field of view. Such a presence of dust covering a low porosity boulder was discounted by previous analysis of the mid-infrared MARA data which did not consider a highly porous boulder as we do here.

Plain Language Summary The Japanese Hayabusa2 space mission returned samples from asteroid Ryugu. Here we compare the spectra of the sample observed in the middle infrared (5–25 μm) with in-situ observations in the part of the electromagnetic spectrum. We find differences between the spectra that can be explained by the presence of fine particles on the surface of Ryugu. Earlier works found that little to no dust can be present on Ryugu and we revisit these studies an derive an upper limit on the amount of dust consistent with the infrared observations. We find that less than 3% of the observed surface can be covered in an opaque dust layer which is likely concentrated in cracks and pores. Our results are consistent with the results of other studies that the amount of dust that a surface of an asteroid can retain decreases with its size.

1. Introduction

The Japanese Hayabusa2 mission to near-Earth asteroid (162173) Ryugu took two sets of samples (A and C) from different sites on Ryugu and returned them to Earth in 2020 (Yada et al., 2022). During its mission, Hayabusa2 investigated the surface Ryugu with four instruments (ONC—camera, NIRS3—near infrared spectrometer, MIR—mid-infrared mapper, and LIDAR—laser altimeter) (Watanabe et al., 2019). Hayabusa2 furthermore deployed the MASCOT lander on the surface, which observed a single boulder of Ryugu in great detail using the MASCAM camera, MASMAG magnetometer and the mid-IR instrument MARA (Ho et al., 2021; Jaumann et al., 2019). Ryugu's surface is covered by dark, highly porous boulders that appear similar to carbonaceous chondrites (CC), in particular CI types (Grott et al., 2019; Kitazato et al., 2019; Sugita et al., 2019). Initial analyses of the returned samples generally support the results of remote sensing and in-situ observations by MASCOT (Nakamura et al., 2023; Yada et al., 2022), whereas detailed comparison of the different observations remains to be done. Here we compare the multi-spectral observations of MARA to the mid-infrared spectrum of sample C0137. MARA is the only instrument of the Hayabusa2 mission that provided observations of Ryugu at several wavelengths in the mid-infrared (MIR, 5–25 μm).

Characteristic minima and maxima in the mid-infrared wavelength region of the electromagnetic spectrum depend on the composition and structure of organic and inorganic materials (e.g., Salisbury et al., 1991). Silicate minerals and silicate-dominated rocks show an emissivity peak known as the Christiansen feature (CF), which is located between 7.5 and 9 μm, and its position is diagnostic of the silicate's crystal structure and indicative of the bulk composition of minerals and rocks. In silicates, fundamental bending and stretching vibrational modes produce diagnostic absorption bands in the ~8–12 and 15–30 μm region (e.g., Lyon, 1965; Salisbury & Walter, 1989; Sandford, 1984).

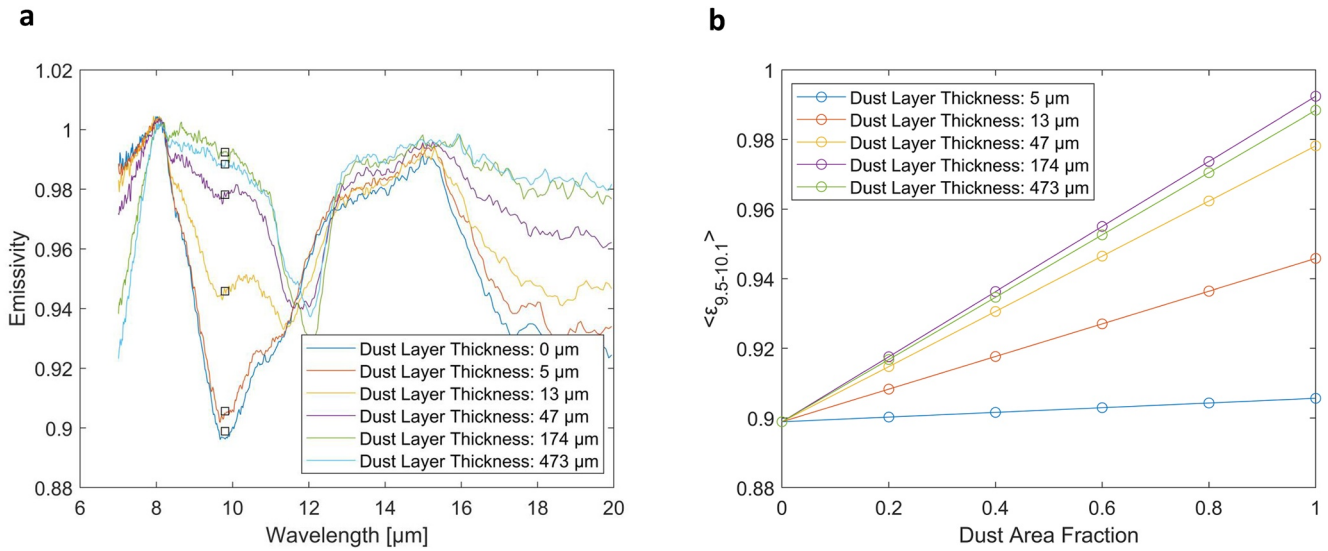

Figure 1. *Influence of basalt dust on the MIR spectra of basalt rock substrate*. (a) Data from Graff (2003) as presented by Hamilton et al. (2021). Spectra are normalized to the maximum around 8 μm. Squares show the average of the spectrum between 9.5 and 10.1 μm. (b) The average spectrum between 9.5 and 10.1 μm for a linear mixture of spectra of dust coated basalt and bare basalt as shown in (a) with varying the area coverage of the dust coating for various dust-layer thicknesses (see Section 4).

The mid-IR spectrum also depends on the physical configuration and particle size of the surface material. For particle sizes comparable to the wavelength of the observation, new features appear due to volume scattering and the contrast of the fundamental vibrational spectral bands is reduced. For silicates, these features occur at wavelengths shorter than the CF and in the interbond region between ~11–13 μm as well as at longer wavelengths (e.g., Aronson & Emslie, 1973; Le Bras & Erard, 2003; Salisbury & Wald, 1992). Thus, the presence of a small amount of dust can influence the observed spectrum as shown in Figure 1 (Hamilton et al., 2021).

2. Methods

2.1. Mid-Infrared Spectroscopy

Particle C0137 was prepared as a polished epoxy mount (Goodrich et al., 2023). We acquired infrared reflectance spectra of the exposed surface using a ThermoScientific Nicolet iN10 Fourier transform infrared microscope at Southwest Research Institute in Boulder, CO. The instrument configuration, calibration, and data processing approach are described by Hamilton (2018) and Hanna et al. (2020); we measured 228 spectra with a spot size of 100 μm^2 per pixel, the average of which is used in this analysis. Additional carbonaceous chondrite samples measured with this spectrometer (e.g., Hamm et al., 2022; Hamilton et al., 2018) are processed in the same manner. The instrument geometry is such that spectra can be inverted via Kirchhoff's Law for comparison with spectra acquired in emission (Ruff et al., 1997; Salisbury et al., 1991). Ideally, spectral comparisons to the Ryugu MARA data would use a library of spectra collected on natural surfaces unaffected by impact ablation, space weathering, or terrestrial alteration, but no such set of samples exists. Most libraries of meteorite spectra have been collected on fine particulates that exhibit band contrast and shape changes attributable to volume scattering (e.g., Figure 1a). Polished samples generally exhibit deeper fundamental bands than cut, natural, or particulate surfaces with no change in spectral shape. As a result, we have chosen to compare the MARA data to a collection of polished samples and describe the impact of this comparison below.

MARA observes the surface of Ryugu through six filters. Two broadband filters allow for a precise temperature measurement (Grott et al., 2019; Hamm et al., 2018) and four narrow band filters to estimate emissivity from 5.5 to 7.0 μm, 8.0 to 9.5 μm, 9.5 to 11.5 μm, and 13.5 to 15.5 μm (Grott et al., 2017). To compare the emissivity obtained with MARA with the laboratory emissivity spectra, the laboratory data ε are resampled over the instrument function τ of each narrow band filter f weighted by the Planck's function $B(\lambda,T)$:

$$\varepsilon_f = \frac{\int \varepsilon(\lambda)\tau_f(\lambda)B(\lambda,T)\mathrm{d}\lambda}{\int \tau_f(\lambda)B(\lambda,T)\mathrm{d}\lambda} \quad (1)$$

where ε_f is the resampled emissivity, temperature T and wavelength λ. The instrument function is described in Hamm et al. (2022). The emissivity for Ryugu was estimated simultaneously with thermal inertia (TI) and surface roughness using data assimilation (Hamm et al., 2022).

2.2. Thermophysical Modeling

For modeling the influence of dust on the diurnal temperature curve we modify the thermal model as reported in Grott et al. (2019) and Hamm et al. (2020). This model is a simplified 1D model and only applicable to the nighttime observations of MARA. The night-time cooling of the diurnal temperature is most sensitive to the presence of dust, whereas the daytime temperature is strongly influenced by roughness effects and reflected sunlight cast by MASCOT into the field of view of MARA (Hamm et al., 2022). The model solves the heat conduction equation assuming a homogenous, opaque layer of variable depth on top of a homogenous half space representing the boulder.

$$\frac{\partial}{\partial t}T(x,t) = \frac{k}{\rho c_p}\frac{\partial^2}{\partial x^2}T(x,t) \tag{2}$$

$$k = \begin{cases} k_d & x \leq x_d \\ k_b & x > x_d \end{cases}$$

Temperature is denoted T, depth x, and time t. The density $\rho = 1{,}800$ kg/m^3 and heat capacity $c_p = 865$ J/K are assumed to be constants as measured for Ryugu samples by Nakamura et al. (2023). The thermal conductivity k is a free parameter of the model, with k_d the thermal conductivity of the dust layer with depth x_d, and k_b the thermal conductivity of the boulder. For the sake of comparability to earlier work the TI is calculated from $\Gamma = \sqrt{k\rho c_p}$ and provided as a proxy parameter. The units of TI are J m^{-2} K^{-1} s$^{-1/2}$ (units are assumed hereafter). The temperature is calculated on a grid of 240 points, with 40 points constituting the dust layer with spacing of grid points increasing by 1.2 from point to point. The total depth of the grid is $20l$, with skin depth

$$l = \sqrt{\frac{k_b}{c_p \rho}\frac{\Omega}{\pi}} \tag{3}$$

where $\Omega = 7.63262\ h$ the rotation period of Ryugu. The upper boundary condition is given by:

$$(1-A)I(t) = (\varepsilon - \zeta)\sigma_B T^4(t)\Big|_{x=0} + k\frac{\partial T(t)}{\partial x}\Big|_{x=0} \tag{4}$$

with Stephan-Boltzmann constant σ_B, bond albedo $A = 0.0146$, and emissivity $\varepsilon = 1$. For calculating the insolation I, the facet orientation of the boulder digital elevation model (DEM) (Hamm et al., 2022) within the MARA field of view is averaged. Reradiation is captured in a factor ζ and subtracted from the bolometric emissivity. This is analogous to assuming that the surrounding surface has on average the same temperature to the modeled surface and ζ would represent the view factor to that surrounding. The factor ζ is tuned in such a way, that the model gives results that are consistent with the simplified thermal model for the boulder DEM as reported in the supplement of Hamm et al. (2022), assuming an emissivity of 1. The best match to the previous simplified model is achieved with $\zeta = 0.11$. At the lower boundary the heat flux is set to zero. The heat conduction equation is solved for 1,000 iterations of Ryugu's rotation. The TI of the boulder, and dust layer thickness was varied in a grid search from, $\Gamma_{\text{boulder}} \in [290{,}420]$, and $x_d \in [5{,}200]$ μm.

For k_d we apply two methods. In the first method, a constant TI of the dust layer is assumed and varied between $\Gamma_{\text{dust}} \in [5{,}125]$. Furthermore, we calculate temperature curves without assuming dustlayer to simulate exposed surfaces of the boulder here the TI is Γ_{bouder} for all x. The upper limit of the dust TI is set at 125. The density of the dust layer is varied between 360, 900, and 1,800 kg/m^3 assuming 80% and 50% and 0% macro-porosity respectively, where 0% would correspond to a top layer with bulk density while the thermal conductivity is reduced by fractures rather than a layer of particles. In the second method, we assume a mean particle size of the dust layer and apply a model relating this particle size to thermophysical parameters. The assumed k_d is related to the dust mean particle size as described in Ryan et al. (2020, 2022), Sakatani et al. (2017) and most recently Persson and

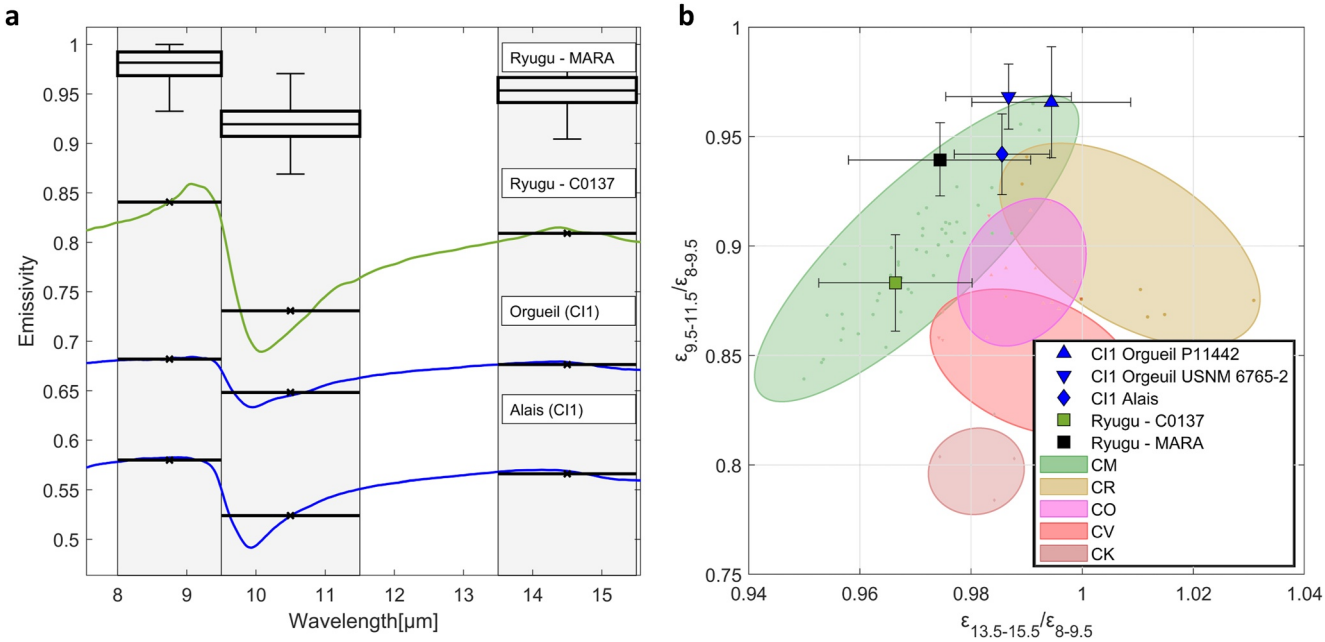

Figure 2. *Comparison of MIR spectrum of C0137 to in-situ observations and CC thin section spectra.* (a) Estimated emissivity of derived from MARA observation, compared to emissivity derived from reflectance spectra of C0137, CI1 Orgueil, and Alais. Spectra are offset for clarity by 0.1, 0.3, and 0.4, respectively. Black horizontal lines are the spectra averaged of the instrument function of the corresponding MARA narrowband filter which are illustrated by gray areas. (b) The ratios of spectra averaged over the MARA bands, B13 and B8 on the *x*-axis, B9 and B8 on the *y*-axis, for thin sections of CI1 chondrites, C0137, and MARA measurements on Ryugu. The error bars for CI1 and C0137 indicate the standard deviation over the band ratios formed from band averages of individual spectra over the sample. The error bars for MARA results indicate the 25th and 75th percentile over the band ratios of emissivity estimates as described in Hamm et al. (2022). Ovals represent band ratios for spectra of thin sections of various types of carbonaceous chondrites as reported in Hamm et al. (2022), data available https://doi.org/10.5281/zenodo.5796141.

Biele (2022). Here will use the latter, as that work is specifically aimed at very fine, loosely packed dust aggregates. Particle size and gravity determine the thermal conductivity and macro-porosity of the layer. We vary the particle size from 1 to 150 μm and set the surface acceleration to 0.01 cm/s^2 consistent with the micro gravity on Ryugu (Kikuchi et al., 2020).

The grid search is refined iteratively starting from a wide range of parameters to properly capture the range of admissible parameter combinations. The last 453 MARA data points measured during the night are used to fit the results of the thermal model for each combinations of parameters. For fitting the data, the W10 filter observations are used which showed the lowest uncertainty (Grott et al., 2019). For each model the χ^2 value is calculated. Parameter combinates with χ^2 values larger than a critical value are discarded. For 450 degrees of freedom, a critical value of 500 corresponds to a 2σ level of confidence.

3. Results

3.1. Comparison of MARA In-Situ, C0137, and Other Laboratory Meteorite Spectra

Figure 2a shows the MARA results and the averaged spectrum of C0137 in comparison to CI1 spectra from Alais and Orgueil. The spectra are shown as measured but with a constant offset in effective emissivity for clarity. The figure also shows the spectra averaged over the MARA bands from around 9, 10, and 14 μm and the MARA emissivity estimates as box plots, with the box defined by the 25th, 50th and 75th percentile, and whiskers indicating the range of outliers. Black horizontal lines indicate the band averages as calculated in Equation 1. The general shapes of the spectra are similar. In all spectra, the maximum emissivity is in the 8–9.5 μm band, emissivity drops in the 9.5–11.5 μm band and increases in the 13.5–15.5 μm band. However, the relative depths of the averages in the 10 and 14 μm bands with respect to the 9 μm band differs between C0137, MARA, and the meteorites, with C0137 plotting lower than the others for the $\varepsilon_{9.5-11.5}/\varepsilon_{8-9.5}$ ratio in Figure 2b.The C0137 spectral features positions are close to those in CI1 chondrite spectra as also shown by T. Nakamura et al. (2023). For C0137, the maximum emissivity peak lies at 9.07 μm and the minimum at 10.05 μm compared to 9.097 and 9.953 μm respectively for CI1 Orgueil.

Figure 2b shows the ratios of the emissivity band averages plotted against each other. Hamm et al. (2022) report the band ratios of 94 spectra taken from thin sections of various types of CC. Figure 2b also shows ovals representing cluster formed by those band ratios of the respective chondrite type. The CI chondrites and CM chondrites form a common cluster of aqueously altered chondrites that is distinct from the other carbonaceous chondrite types. C0137 is situated within the cluster of aqueously altered CM types but shows greater contrast in the 9.5–11.5 band relative to the CI1 meteorites. The band ratios observed by MARA overlap with the CI1 band ratios. The $\varepsilon_{13.5–15.5}/\varepsilon_{8–9.5}$ ratio for C0137 is consistent with the in-situ results obtained with MARA. The $\varepsilon_{9.5–11.5}/\varepsilon_{8–9.5}$ ratio is smaller by a few percent for C0137, indicating a larger contrast between the maximum and minimum of the spectrum compared to MARA observations.

Whereas the C0137 spectrum is measured on a polished, interior surface of a Ryugu particle, the MARA spectrum is measured on a natural boulder surface with a thin dust deposit, characteristics that are expected to reduce spectral contrast on Ryugu. The $\varepsilon_{9.5–11.5}/\varepsilon_{8–9.5}$ ratio for the C0137 spectrum is also substantially lower than for CI1 meteorites, even though all are polished sections, likely due to the effects of terrestrial weathering and contamination on the meteorites' spectra. In other words, we expect that pristine CI1 meteorite spectra would have band ratios resembling C0137, based on the interpretation that Ryugu particles represent pristine CI1 material (Yokoyama et al., 2023). Finally, the fact that the MARA band ratios are comparable to those of the CI1 meteorites is consistent with comparing a natural Ryugu surface with to polished meteorites that exhibit shallower features due to weathering and contamination.

3.2. Upper Limit on Dust Layer

Although the presence of dust could explain the lower $\varepsilon_{9.5–11.5}/\varepsilon_{8–9.5}$ ratio of C0137, the presence of dust within the MARA field of view that would mask the higher TI of the boulder was discarded in earlier studies (Grott et al., 2019). However, that work did not test the upper limit of the thickness of dust assuming a porous boulder with low TI. In this study we find that the range of possible combinations of dust deposit TI and depth is very narrow. The widest range of permissible combinations of dust TI and deposit thickness is for a boulder TI of 305. The results are shown in Figure 3a. For a dust TI of 125 the layer must be thinner than 65 μm. The maximum depth of dust decreases with lower TI and is smaller than 10 μm for an assumed dust TI of 50. The assumed dust TI can be related to the dust mean particle size as described in Section 2.2. We arrive at a relation of dust particle size and dust TI $D(\Gamma)$ as shown in Figure 3a. In all cases the acceptable range of dust thickness is smaller than the corresponding particle size. Furthermore, Figure 3a shows the results assuming no macro-porosity for the dust layer, and range of fitting parameters drastically decreases drastically with increasing porosity. Consequently, a homogenous dust layer in the MARA field of view seems very unlikely.

We thus test the thermal model using thermophysical parameters as a function of particle size as in Persson and Biele (2022) and assume a discontinuous dust layer by converting the model temperatures to flux observed by MARA F and assuming that only a fraction of the field of view (f_{dust}) covered by dust: $F = f_{\mathrm{dust}}\, F(T_{\mathrm{dust}}) + (1 - f_{\mathrm{dust}})\, F(T_{\mathrm{rock}})$. We vary the area fraction of the dust cover from 0 to 1, the dust TI and the thickness of the dust cover, the TI of the rock is fixed at 305. Figure 3b shows the parameter combinations that fit the nighttime data as in Figure 3a, with the dust layer thickness fixed at 150 μm. Here we find that there are combinations where the particle size of the dust layer is smaller than the dust layer itself. The black line showing the particle size such for which the dust layer can be made up of five layers of particles, from which the dust layer can be assumed a homogenous layer in a 1D thermophysical model (Biele et al., 2019). We find similar results for various values of x_d, with 150 μm is showing the largest acceptable area fraction of dust, which in all cases is below 3%.

4. Discussion

The mid-IR spectrum of C0137 shows features with positions that are generally consistent with CI1 chondrites and the spectra of other Ryugu samples reported by Nakamura et al. (2023). However, the band ratios for C0137 are significantly different from the ratios found for the CI1 chondrites, mainly due to the lower contrast of the chondrites' spectra. As indicated by the large error bars in Figure 2b, the variance over the samples is large. Furthermore, two examples of the CI1 Orgueil differ from each other, within that variance. The two available CI chondrites, Alais and Orgueil, were exposed to substantial terrestrial alteration such that they might not be the best representatives of their type. With such few CI samples measured it is furthermore unclear whether MARA

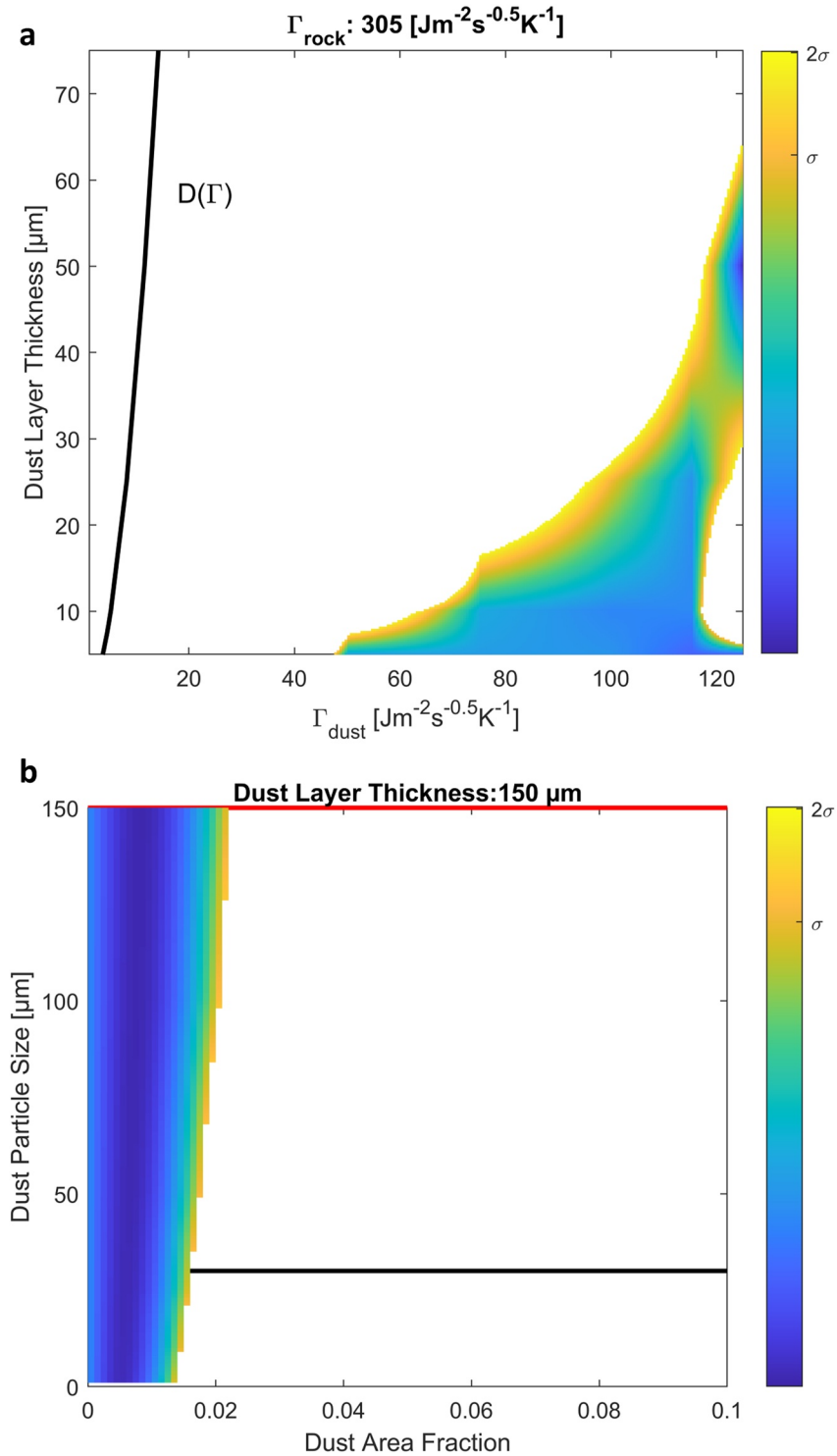

Figure 3. *The influence of a dust layer on temperature observations* (a) Parameter combinations of the two-layer thermal model resulting in nighttime temperatures consistent with brightness temperatures observed by MARA assuming the dust covers the entire MARA FoV. Color indicates χ^2 values and their corresponding level of significance. Here thermal inertia (TI) of the rock is fixed to 305. *Y*-axis shows dust layer thickness and *x*-axis is assumed TI of the dust. The dust particle size as a function of the dust TI is shown as a black line plot, based on Persson and Biele (2022). (b) Similar to (a) with the dust covering a variable fraction of the MARA FoV, and using the dependency of TI on particle size and temperature in the thermal model. Acceptable parameter combinations are plotted against dust area fraction, and particle size, for a fixed dust layer thickness of 150 µm. Horizontal lines indicate the thickness of the dust layer 150 µm (red) and particle size where the dust layer constituted of five layers of particles 30 µm (black).

could distinguish CI and CM group meteorites. The spectral variance over the different Ryugu samples could be significant and with more MIR spectra of these samples becoming available in the future a better quantification of the variance will be feasible. The spectra reported in Nakamura et al. (2023) show a significant spectral feature from the sapphire window of their setup that drastically influences the MARA band averages. A comparison would be misleading without a proper correction.

Nevertheless, the difference between the $\varepsilon_{9.5–11.5}/\varepsilon_{8–9.5}$ ratio observed by MARA and calculated for C0137 could be well explained by the presence of a small amount of dust on the observed boulder. Work by Graff (2003) (as cited by Hamilton et al., 2021 in the analysis of Bennu spectra) shows that as little as 13 μm of dust coating can change the spectral properties of the substrate in mid-IR significantly. Figure 1a shows dust-coated rock spectra. The average of the minimum at 9.5–10.1 μm is plotted as squares and that strongly affected by the presence of dust, whereas the region from 13.5 to 15.5 μm is much less affected. This offers an explanation why the $\varepsilon_{9.5–11.5}/\varepsilon_{8–9.5}$ ratio is significantly different for C0137 while the $\varepsilon_{13.5–15.5}/\varepsilon_{8–9.5}$ ratio is consistent with the MARA observations. Note that this effect depends on the composition of the dust and substrate materials such that for the material of Ryugu the effect could be less or more pronounced.

Thermal modeling reveals that a discontinuous dust layer better fits the data than a homogenous cover. Assuming thermophysical properties of the dust layer, consistent with loose, fine particles, only a discontinuous dust cover covering less than 3% can be fitted to the data. We produce linear mixtures of the dust covered spectra: $\varepsilon_{\mathrm{mix}}(\lambda) = f_{\mathrm{dust}}\,\varepsilon_{\mathrm{dust}}(\lambda) + (1 - f_{\mathrm{dust}})\,\varepsilon_{\mathrm{rock}}(\lambda)$ and the average spectrum around the minimum is shown in Figure 1b and although the effect is smaller, the required few percent of change can be obtained below 10% dust area coverage. However, the 3% area coverage obtained for an opaque dust layer is not enough to explain the full discrepancy between C0137 spectrum and MARA observations. Due to the limitation of our model which assumes an opaque dust layer, dust layers of very few or single particles thick and thus transparent in mid-IR cannot be captured by the model and could cover the entire MARA field of view. While the exact thermophysics of such thin, transparent layers of dust particles are not yet well understood they should have temperatures more similar to the boulder while still reducing the CF due to scattering. For example, basalt dust shown in Figure 1 is mostly consisting of dust particles with 5–50 μm in size, corresponding to a TI of about 10. Figure 1 shows that the 13 μm thick dustlayer, consisting of 1–2 layers of particles, shows a significant reduction of the CF.

Our analysis reinforced previous results that no combination of TI of dust and dust layer thickness can explain the MARA observations when a higher TI than 325 is assumed. In particular, a TI of 890 as reported for the Ryugu samples (Nakamura et al., 2023) can be excluded as a TI for the observed boulder. This discrepancy is not yet understood with one possibility being that a high degree of fracturing in the boulder rather than high porosity obstructs the heat conduction into its interior (Ishizaki et al., 2023). The fragments obtained after the destructive sampling procedure could then have a higher TI than the fragmented aggregate.

5. Conclusions

Multi-spectral observations of Ryugu by the MARA instrument are largely consistent with the Ryugu sample C0137 from the second sampling site and those of CI chondrites. However, the reduced spectral contrast between the maximum around 9 μm and the minimum at 10 μm in the MARA data could be indicative of a small amount of dust on the surface of Ryugu, as this part of the spectrum is particularly sensitive to the presence of dust. Using a 2-layer thermophysical model, we investigate the presence of a dust-layer on Ryugu as an explanation for the difference between C0137 and MARA observations. Within the assumption of the model, that is, an opaque, homogenous dustlayer, we can exclude a dust-layer covering the full field of view of MARA, while assuming thermal conductivity and porosity typical for a layer of loose, fine particles in micro-gravity. Such an opaque, homogeneous dustlayer cannot cover more than 3% of the MARA field of view, and this is not enough to explain the difference between MARA observations and C0137. A semi-transparent layer of very few dust particles in thickness cannot be covered by our model and thus not be ruled out, but could still contribute significantly to the reduction of the CF. Some models assuming for the top layer a higher TI $20 < \Gamma < 125$ and bulk porosity of the boulder can fit the data. This means one or a combination of the following scenarios:

1. Fine dust is concentrated in crevices and cracks;
2. The remainder of the MARA field of view is devoid of dust or covered by a semi-transparent dust layer, for example, a monolayer of dust particles;
3. The dust could be cemented to some extent, thus increasing the TI of the layer

The results are consistent with the general trend that small asteroids lack fine regolith and the dust produced on such objects is lost quickly (Hsu et al., 2022). A diameter of 1 km is a typical size below which asteroids tend to lose most of the surface fines, and Ryugu's diameter is in that range (Watanabe et al., 2019). Furthermore, work by Cambioni et al. (2021) suggest that the high porosity of Ryugu's materials reduces the amount of dust produced by impacts or thermal cracking. The scenario that small amounts of dust amassing in cracks and crevices on the irregular shaped boulder, whereas most of the boulder surface is bare rock, reconciles observations of mobilization of fine particles during the sampling operations to those of MASCOT that did not observe fine particles on boulders. Hayabusa2's thrusters changed the albedo of some boulders which was interpreted as brushing off dust from cracks and pores (Morota et al., 2020).

Data Availability Statement

The thermal model and fitting routines to produce the here-presented results are publicly available in Hamm et al. (2023). The new data presented for C0137 as well as the variability of the CI spectra are available in the same repository together with the MARA data. Band ratios of meteorite thin sections are available in the Zenodo repository 5796141 (Hamm et al., 2021) as presented in Hamm et al. (2022). The MARA data can also be downloaded as a PDS4 Bundle in Grott et al. (2023). The data for the basalt dust spectra is from Graff (2003) as presented by Hamilton et al. (2021) and available here: http://speclib.asu.edu. Proceed using the guest-login and download the spectra number 659 and 715–719.

Acknowledgments
M.H. is funded by the Deutsche Forschungsgemeinschaft (DFG, German Research Foundation)—Project-No. 497966340. C.G. acknowledges support from the Lunar and Planetary Institute (USRA-Houston). LPI Contribution No. 3022. LPI is operated by the Universities Space Research Association. We are grateful to JAXA for the allocation of Ryugu particle C0137. We thank Dr. J. Biele for providing the data of his and Dr. B.N.J. Persson's thermal conductivity model and his help in implementing it. We thank the reviewers, Dr. A. Ryan and an anonymous reviewer, for their helpful comments. Open Access funding enabled and organized by Projekt DEAL.

References

Aronson, J. R., & Emslie, A. G. (1973). Spectral reflectance and emittance of particulate materials. 2: Application and results. *Applied Optics, AO*, *12*(11), 2573–2584. https://doi.org/10.1364/AO.12.002573

Biele, J., Kührt, E., Senshu, H., Sakatani, N., Ogawa, K., Hamm, M., et al. (2019). Effect of dust layers on thermal emission from airless bodies. *Progress in Earth and Planetary Science*, *6*(1), 48. https://doi.org/10.1186/s40645-019-0291-0

Cambioni, S., Delbo, M., Poggiali, G., Avdellidou, C., Ryan, A. J., Deshapriya, J. D. P., et al. (2021). Fine-regolith production on asteroids controlled by rock porosity. *Nature*, *598*(7879), 49–52. https://doi.org/10.1038/s41586-021-03816-5

Goodrich, C., Lee, S., Mane, P., Hamilton, V. E., Zolensky, M. E., Kita, N. T., et al. (2023). Ryugu and the quest for unaltered CI-like materials from the early solar system. *LPSC*, *54*, #1446.

Graff, T. G. (2003). Effects of dust coatings on visible, near-infrared, thermal emission, and Mossbauer spectra: Implications for mineralogical remote sensing of Mars (M.S. Thesis). Arizona State University.

Grott, M., Knollenberg, J., Borgs, B., Hänschke, F., Kessler, E., Helbert, J., et al. (2017). The MASCOT radiometer MARA for the Hayabusa 2 Mission. *Space Science Reviews*, *208*(1–4), 413–431. https://doi.org/10.1007/s11214-016-0272-1

Grott, M., Knollenberg, J., Hamm, M., Borgs, B., Hänschke, F., Kessler, E., et al. (2023). Hayabusa2 MASCOT MARA Radiometer Bundle, urn:jaxa:darts:hyb2_mascot_mara [Dataset]. JAXA Data Archives and Transmission System. https://doi.org/10.17597/isas.darts/hyb2-01000

Grott, M., Knollenberg, J., Hamm, M., Ogawa, K., Jaumann, R., Otto, K. A., et al. (2019). Low thermal conductivity boulder with high porosity identified on C-type asteroid (162173) Ryugu. *Nature Astronomy*, *3*(11), 971–976. https://doi.org/10.1038/s41550-019-0832-x

Hamilton, V. E. (2018). Spectral classification of ungrouped carbonaceous chondrites I: Data collection and processing. *Lunar and Planetary Science Conference*, *49*, #1759.

Hamilton, V. E., Abreu, N. M., Bland, P. A., Connolly, H. C., Jr., Hanna, R. D., Lauretta, D. S., et al. (2018). Spectral classification of ungrouped carbonaceous chondrites II: Parameters and comparison to independent measures. *Lunar and Planetary Science Conference*, *49*, #1753.

Hamilton, V. E., Christensen, P. R., Kaplan, H. H., Haberle, C. W., Rogers, A. D., Glotch, T. D., et al. (2021). Evidence for limited compositional and particle size variation on asteroid (101955) Bennu from thermal infrared spectroscopy. *Astronomy & Astrophysics*, *650*, A120. https://doi.org/10.1051/0004-6361/202039728

Hamm, M., Grott, M., Kührt, E., Pelivan, I., & Knollenberg, J. (2018). A method to derive surface thermophysical properties of asteroid (162173) Ryugu (1999JU3) from insitu surface brightness temperature measurements. *Planetary and Space Science*, *159*, 1–10. https://doi.org/10.1016/j.pss.2018.03.017s

Hamm, M., Grott, M., Senshu, H., Knollenberg, J., de Wiljes, J., Hamilton, V. E., et al. (2021). Data assimilation of MASCOT radiometer data [Dataset]. Zenodo Repository 5796141. https://doi.org/10.5281/zenodo.5796141

Hamm, M., Grott, M., Senshu, H., Knollenberg, J., de Wiljes, J., Hamilton, V. E., et al. (2022). Mid-infrared emissivity of partially dehydrated asteroid (162173) Ryugu shows strong signs of aqueous alteration. *Nature Communications*, *13*(1), 364. https://doi.org/10.1038/s41467-022-28051-y

Hamm, M., Hamilton, V. E., & Goodrich, C. A. (2023). Model and data: Evidence for the presence of thin dust deposits on Ryugu's boulders from Hayabusa2 MARA and sample data [Dataset]. Figshare. https://doi.org/10.6084/m9.figshare.23275805.v1

Hamm, M., Pelivan, I., Grott, M., & de Wiljes, J. (2020). Thermophysical modelling and parameter estimation of small Solar system bodies via data assimilation. *Monthly Notices of the Royal Astronomical Society*, *496*(3), 2776–2785. https://doi.org/10.1093/mnras/staa1755

Hanna, R. D., Hamilton, V., Haberle, C., King, A., Abreu, N., & Friedrich, J. (2020). Distinguishing relative aqueous alteration and heating among CM chondrites with IR spectroscopy. *Icarus*, *346*, 113760. https://doi.org/10.1016/j.icarus.2020.113760

Ho, T.-M., Jaumann, R., Bibring, J. P., Grott, M., Glaßmeier, K. H., Moussi, A., et al. (2021). The MASCOT lander aboard Hayabusa2: The in-situ exploration of NEA (162173) Ryugu. *Planetary and Space Science*, *200*, 105200. https://doi.org/10.1016/j.pss.2021.105200

Hsu, H. W., Wang, X., Carroll, A., Hood, N., & Horányi, M. (2022). Fine-grained regolith loss on sub-km asteroids. *Nature Astronomy*, *6*(9), 1043–1050. https://doi.org/10.1038/s41550-022-01717-9

Ishizaki, T., Nagano, H., Tanaka, S., Sakatani, N., Nakamura, T., Okada, T., et al. (2023). Measurement of microscopic thermal diffusivity distribution for Ryugu sample by infrared lock-in periodic heating method. *International Journal of Thermophysics*, *44*(4), 51. https://doi.org/10.1007/s10765-023-03158-6

Jaumann, R., Schmitz, N., Ho, T. M., Schröder, S. E., Otto, K. A., Stephan, K., et al. (2019). Images from the surface of asteroid Ryugu show rocks similar to carbonaceous chondrite meteorites. *Science*, *365*(6455), 817–820. https://doi.org/10.1126/science.aaw8627

Kikuchi, S., Watanabe, S.-I., Saiki, T., Yabuta, H., Sugita, S., Morota, T., et al. (2020). Hayabusa2 landing site selection: Surface topography of Ryugu and touchdown safety. *Space Science Reviews*, *216*(7), 116. https://doi.org/10.1007/s11214-020-00737-z

Kitazato, K., Milliken, R. E., Iwata, T., Abe, M., Ohtake, M., Matsuura, S., et al. (2019). The surface composition of asteroid 162173 Ryugu from Hayabusa2 near-infrared spectroscopy. *Science*, *364*(6437), eaav7432. https://doi.org/10.1126/science.aav7432

Le Bras, A., & Erard, S. (2003). Reflectance spectra of regolith analogs in the mid-infrared: Effects of grain size. *Planetary and Space Science*, *51*(4–5), 281–294. https://doi.org/10.1016/S0032-0633(03)00017-5

Lyon, R. J. P. (1965). Analysis of rocks by spectral infrared emission (8 to 25 microns). *Economic Geology*, *60*(4), 715–736. https://doi.org/10.2113/gsecongeo.60.4.715

Morota, T., Sugita, S., Cho, Y., Kanamaru, M., Tatsumi, E., Sakatani, N., et al. (2020). Sample collection from asteroid (162173) Ryugu by Hayabusa2: Implications for surface evolution. *Science*, *368*(6491), 654–659. https://doi.org/10.1126/science.aaz6306

Nakamura, T., Matsumoto, M., Amano, K., Enokido, Y., Zolensky, M. E., Mikouchi, T., et al. (2023). Formation and evolution of carbonaceous asteroid Ryugu: Direct evidence from returned samples. *Science*, *379*(6634), eabn8671. https://doi.org/10.1126/science.abn8671

Persson, B. N. J., & Biele, J. (2022). Heat transfer in granular media with weakly interacting particles. *AIP Advances*, *12*(10), 105307. https://doi.org/10.1063/5.0108811

Ruff, S. W., Christensen, P. R., Barbera, P. W., & Anderson, D. L. (1997). Quantitative thermal emission spectroscopy of minerals: A laboratory technique for measurement and calibration. *Journal of Geophysical Research*, *102*(B7), 14899–14913. https://doi.org/10.1029/97JB00593

Ryan, A. J., Pino Muñoz, D., Bernacki, M., & Delbo, M. (2020). Full-field modeling of heat transfer in asteroid regolith: 1. Radiative thermal conductivity of polydisperse particulates. *Journal of Geophysical Research: Planets*, *125*(2), e2019JE006100. https://doi.org/10.1029/2019JE006100

Ryan, A. J., Pino Muñoz, D., Bernacki, M., Delbo, M., Sakatani, N., Biele, J., et al. (2022). Full-field modeling of heat transfer in asteroid regolith: 2. Effects of porosity. *Journal of Geophysical Research: Planets*, *127*(6), e2022JE007191. https://doi.org/10.1029/2022JE007191

Sakatani, N., Ogawa, K., Iijima, Y., Arakawa, M., Honda, R., & Tanaka, S. (2017). Thermal conductivity model for powdered materials under vacuum based on experimental studies. *AIP Advances*, *7*(1), 015310. https://doi.org/10.1063/1.4975153

Salisbury, J. W., & Wald, A. (1992). The role of volume scattering in reducing spectral contrast of reststrahlen bands in spectra of powdered minerals. *Icarus*, *96*(1), 121–128. https://doi.org/10.1016/0019-1035(92)90009-V

Salisbury, J. W., & Walter, L. S. (1989). Thermal infrared (2.5–13.5 μm) spectroscopic remote sensing of igneous rock types on particulate planetary surfaces. *Journal of Geophysical Research*, *94*(B7), 9192–9202. https://doi.org/10.1029/JB094iB07p09192

Salisbury, J. W., Walter, L. S., Vergo, N., & D'Aria, D. M. (1991). *Infrared (2.1-25 um) spectra of minerals*. The Johns Hopkins University Press.

Sandford, S. A. (1984). Infrared transmission spectra from 2.5 to 25 μm of various meteorite classes. *Icarus*, *60*(1), 115–126. https://doi.org/10.1016/0019-1035(84)90141-6

Sugita, S., Honda, R., Morota, T., Kameda, S., Sawada, H., Tatsumi, E., et al. (2019). The geomorphology, color, and thermal properties of Ryugu: Implications for parent-body processes. *Science*, *364*(6437), eaaw0422. https://doi.org/10.1126/science.aaw0422

Watanabe, S., Hirabayashi, M., Hirata, N., Hirata, N., Noguchi, R., Shimaki, Y., et al. (2019). Hayabusa2 arrives at the carbonaceous asteroid 162173 Ryugu - A spinning top–shaped rubble pile. *Science*, *364*(6437), eaav8032. https://doi.org/10.1126/science.aav8032

Yada, T., Abe, M., Okada, T., Nakato, A., Yogata, K., Miyazaki, A., et al. (2022). Preliminary analysis of the Hayabusa2 samples returned from C-type asteroid Ryugu. *Nature Astronomy*, *6*(2), 214–220. https://doi.org/10.1038/s41550-021-01550-6

Yokoyama, T., Nagashima, K., Nakai, I., Young, E. D., Abe, Y., Aléon, J., et al. (2023). Samples returned from the asteroid Ryugu are similar to Ivuna-type carbonaceous meteorites. *Science*, *379*(6634), eabn7850. https://doi.org/10.1126/science.abn7850